frontiers | Frontiers in Bioengineering and Biotechnology

TYPE Original Research
PUBLISHED 07 March 2024
DOI 10.3389/fbioe.2024.1372688

OPEN ACCESS

EDITED BY
Xin Su,
Beijing University of Chemical Technology, China

REVIEWED BY
Mingchang Wang,
Jilin University, China
Shihui Wang,
Beijing University of Chemical Technology, China
Jianxun Ding,
Chinese Academy of Sciences (CAS), China

*CORRESPONDENCE
Meng Han,
meng68527@126.com
Yimin Wang,
drwangyimin@hebmu.edu.cn

†These authors have contributed equally to this work

RECEIVED 18 January 2024
ACCEPTED 19 February 2024
PUBLISHED 07 March 2024

CITATION
Feng K, Di Y, Han M, Yan W, Guo Y, Huai X and Wang Y (2024), A photoelectrochemical aptasensor based on double Z-scheme α-Fe_2O_3/MoS_2/Bi_2S_3 ternary heterojunction for sensitive detection of circulating tumor cells. *Front. Bioeng. Biotechnol.* 12:1372688. doi: 10.3389/fbioe.2024.1372688

A photoelectrochemical aptasensor based on double Z-scheme α-Fe_2O_3/MoS_2/Bi_2S_3 ternary heterojunction for sensitive detection of circulating tumor cells

Kai Feng[1†], Ya Di[1†], Meng Han[1]*, Weitao Yan[1], Yulin Guo[1], Xiangqian Huai[2] and Yimin Wang[1]*

[1]The First Hospital of Qinhuangdao, Qinhuangdao, China, [2]College of Food Science and Technology, Hebei Agricultural University, Baoding, China

A novel photoelectrochemical (PEC) aptasensor based on a dual Z-scheme α-Fe_2O_3/MoS_2/Bi_2S_3 ternary heterojunction for the ultrasensitive detection of circulating tumor cells (CTCs) was developed. The α-Fe_2O_3/MoS_2/Bi_2S_3 nanocomposite was prepared via a step-by-step route, and the photoproduced electron/hole transfer path was speculated by conducting trapping experiments of reactive species. α-Fe_2O_3/MoS_2/Bi_2S_3-modified electrodes exhibited greatly enhanced photocurrent under visible light due to the double Z-scheme charge transfer process, which met the requirement of the PEC sensor for detecting larger targets. After the aptamer was conjugated on the photoelectrode through chitosan (CS) and glutaraldehyde (GA), when MCF-7 cells were presented and captured, the photocurrent of the PEC biosensing system decreased due to steric hindrance. The current intensity had a linear relationship with the logarithm of MCF-7 cell concentration ranging from 10 to 1×10^5 cells mL^{-1}, with a low detection limit of 3 cell mL^{-1} (S/N = 3). The dual Z-scheme α-Fe_2O_3/MoS_2/Bi_2S_3 ternary heterojunction-modified PEC aptasensor exhibited high sensitivity and excellent specificity and stability. Additionally, MCF-7 cells in human serum were determined by this PEC aptasensor, exhibiting great potential as a promising tool for clinical detection.

KEYWORDS

photoelectrochemical aptasensor, dual Z-scheme, α-Fe_2O_3/MoS_2/Bi_2S_3 ternary heterojunction, aptamer, circulating tumor cells

1 Introduction

Circulating tumor cells (CTCs) are a dependable biomarker for cancer diagnosis, detection, and prediction. They are released from primary or metastatic sites of tumors and circulate through peripheral blood to distant body regions (Hong and Zu, 2013; Tang et al., 2016; Wang et al., 2023a; Gong et al., 2023). Quick, inexpensive, and highly sensitive techniques to identify CTCs are urgently needed. Various conventional strategies have been established for the detection of CTCs including the immunomagnetic bead approach (Den Toonder, 2011), reverse transcriptase polymerase chain reaction (RT-PCR)-based

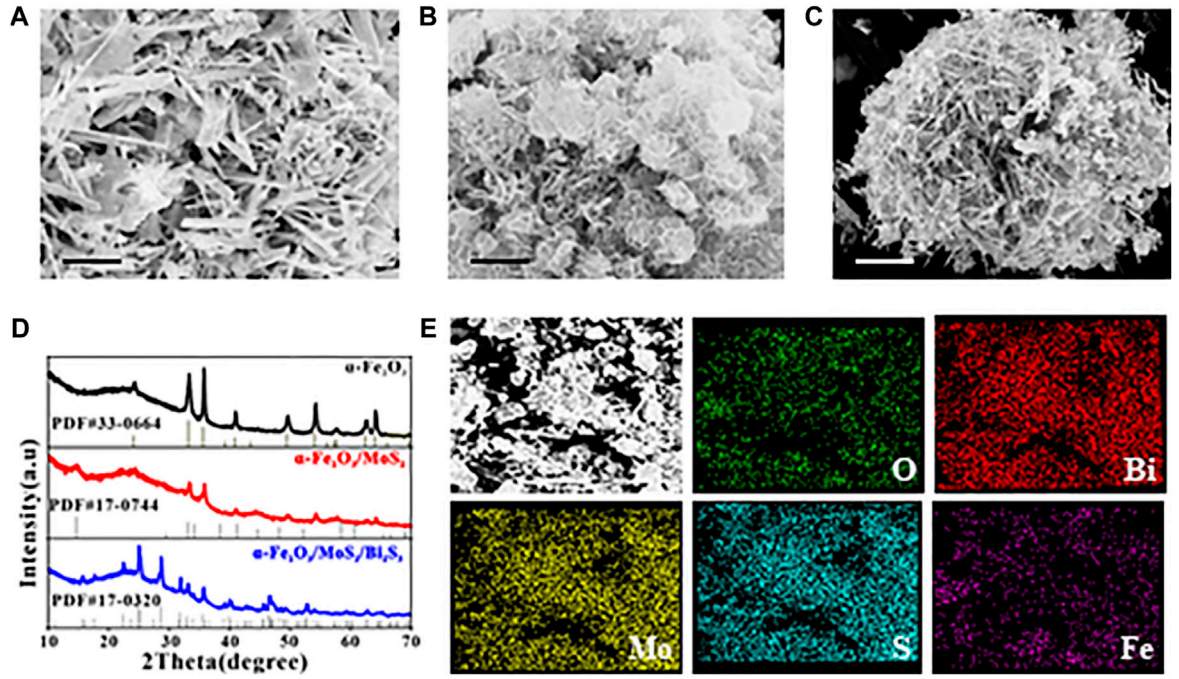

FIGURE 1
SEM images of **(A)** α-Fe_2O_3, **(B)** α-Fe_2O_3/MoS_2, and **(C)** α-Fe_2O_3/MoS_2/Bi_2S_3. **(D)** XRD patterns of α-Fe_2O_3, α-Fe_2O_3/MoS_2, and α-Fe_2O_3/MoS_2/Bi_2S_3. **(E)** SEM-EDS mapping of α-Fe_2O_3/MoS_2/Bi_2S_3. Scale bar for **(A–C)** is 1 μm.

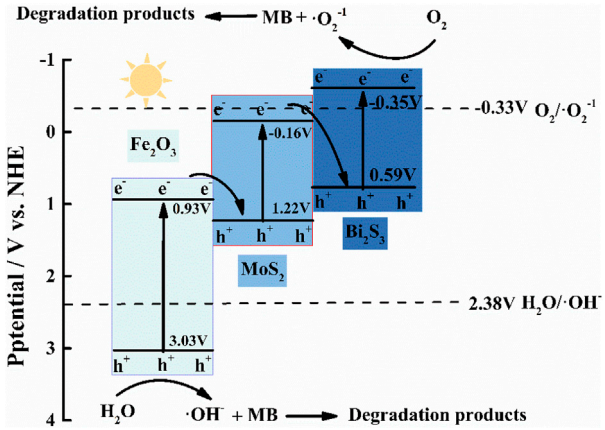

FIGURE 2
Proposed charge transfer and photocatalytic mechanisms of the double Z-scheme α-Fe_2O_3/MoS_2/Bi_2S_3 ternary heterojunction.

technique (Dirix et al., 2009), enzyme-linked immunosorbent immunoassay (ELISA) (Van der Auwera et al., 2010), and fluorescence spectroscopy (Yang et al., 2018). Nevertheless, complicated operations, expensive instruments, and low sensitivity limit these methods for CTC-based clinical diagnostics. The photoelectrochemical (PEC) aptasensor, as a novel and quickly evolving technique, has found widespread use in trace analyses as an efficient method. The PEC aptasensor delivers reasonable specificity between the aptamers and target analytes (Zhong et al., 2023). As "chemical antibodies," aptamers are single-stranded oligonucleotide sequences synthesized from the SELEX process (Stoltenburg et al., 2007; Fang and Tan, 2010; Yi et al., 2023; Zhao et al., 2023). Meanwhile, the PEC aptasensor has a high sensitivity because the excitation light source and current signal are separated completely, which minimizes interference between the input and output signals (Osterloh, 2013). Additionally, the PEC aptasensor offers exceptional benefits including simplicity, low cost, and easy integration by integrating a relatively simple optical and electrochemical instrument (Freeman et al., 2013; Yue et al., 2013). However, in order to achieve the very sensitive detection of CTCs, PEC aptasensors require a strong photocurrent because of the dielectric and relatively large size of CTCs.

Currently, semiconductors are preferred as photoactive materials for the PEC aptasensor because of their exceptional photocurrent enhancement. Molybdenum disulfide (MoS_2) is a typical photoactive material, which has a band gap is approximately 1.8 eV (Wu et al., 2017) and energy levels that match the visible region of the solar spectrum, making it efficient for visible-light harvesting (Li et al., 2011; Hong et al., 2014). However, the challenges related to undesired photo-generated carrier (electron/hole, e−/h+) lifetimes may limit its PEC performance (Pei et al., 2019). Constructing a heterostructure (or heterojunction) with other semiconductors is considered the most efficient strategy (Liu et al., 2017; Han et al., 2018). To further boost the light utilization and electron–hole pair separation, Z-scheme heterojunction has been carried out using multiple semiconductors with well-matched band structures, which exhibits a distinct photocatalytic redox ability (Saravanakumar and Park, 2021; Yu et al., 2021). Bismuth trisulfide (Bi_2S_3), with a direct band gap (1.3–1.7 eV), is also ideally suited to absorb visible light and

10.3389/fbioe.2024.1372688

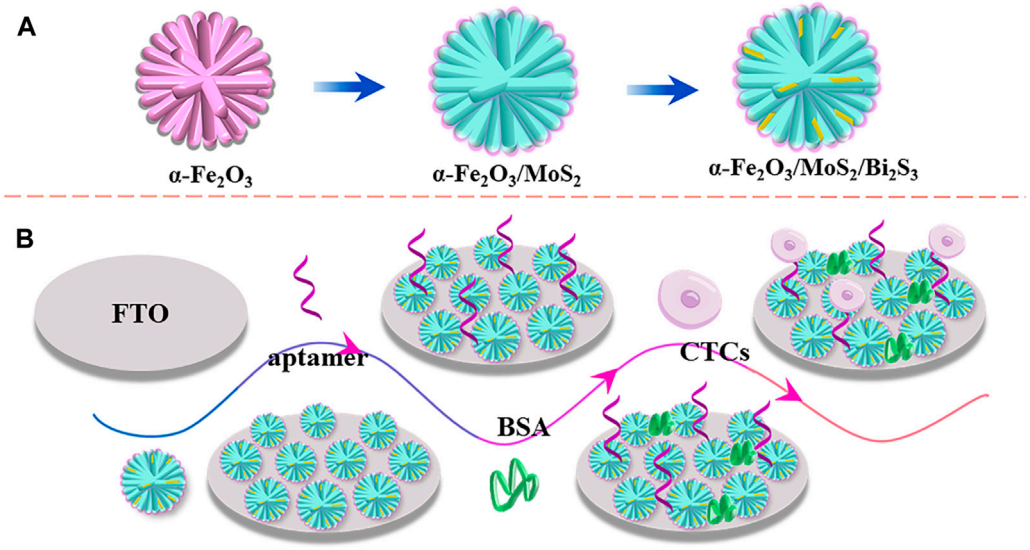

SCHEME 1
Schemata of the preparation of the α-Fe_2O_3/MoS_2/Bi_2S_3 ternary heterojunction **(A)** and fabrication of the PEC aptasensor **(B)**.

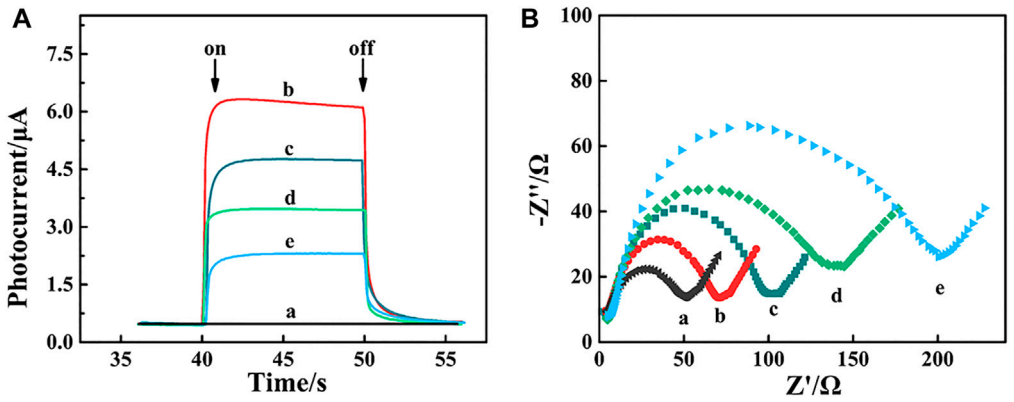

FIGURE 3
Photocurrent response **(A)** and EIS spectrum **(B)** of FTO electrode. (a), α-Fe_2O_2/MoS_2/Bi_2S_2 heterojunction (b), α-Fe_2O_2/MoS_2/Bi_2S_2 heterojunction/Apt-DNA (c) and α-Fe_2O_3/MoS_2/Bi_2S_3 /Apt-DNA/BSA (d) and α-Fe_2O_2/MoS_2/Bi_2S_2/Apt-DNA/BSA/MCF-7 cell.

particularly well-matched with MoS_2 nanosheets for the construction of Z-scheme heterojunction in PEC analysis. For example, Q.A. Drmosh prepared Z-scheme Bi_2S_3/MoS_2/TiO_2 nanotube-based photoelectrodes with enhanced visible light absorption and increased charge lifetime (Wang Q. et al., 2023). Similarly, hematite (α-Fe_2O_3), with its band gap (1.9–2.2 eV), nontoxic nature, and excellent and chemical stability, is also a promising photocatalyst in the visible-light region (Zhang Z. et al., 2020; Wheeler et al., 2012). In photocatalysis, the combination of α-Fe_2O_3 and MoS_2 (α-Fe_2O_3/MoS_2) is also a suitable candidate to use as a Z-scheme heterojunction. Guo and Xing designed a hollow flower-like polyhedral α-Fe_2O_3/MoS_2/Ag Z-scheme heterojunction that demonstrated excellent photocatalytic degradation for 2,4-DCP (Guo et al., 2020). To enhance the activity of Z-scheme photocatalysts even more, the double Z-scheme photocatalytic system coupling of three or more semiconductors has gained extensive attention in photocatalysts, which enhanced visible light absorption and achieved more efficient charge carrier separation and transfer (Jiang et al., 2018).

Herein, we presented a novel PEC aptasensor based on a dual Z-scheme α-Fe_2O_3/MoS_2/Bi_2S_3 ternary heterojunction for the ultrasensitive detection of CTCs. The α-Fe_2O_3/MoS_2/Bi_2S_3 nanocomposite was prepared via a step-by-step route, and α-Fe_2O_3/MoS_2/Bi_2S_3-modified electrodes exhibited greatly enhanced photocurrent under visible light. The photoproduced electron/hole transfer path was speculated by conducting trapping experiments of reactive species to demonstrate the charge transfer process. After the aptamer was conjugated on the photoelectrode, MCF-7 cells were captured through a specific immunoreaction between the aptamer and tumor, leading to the decrease in

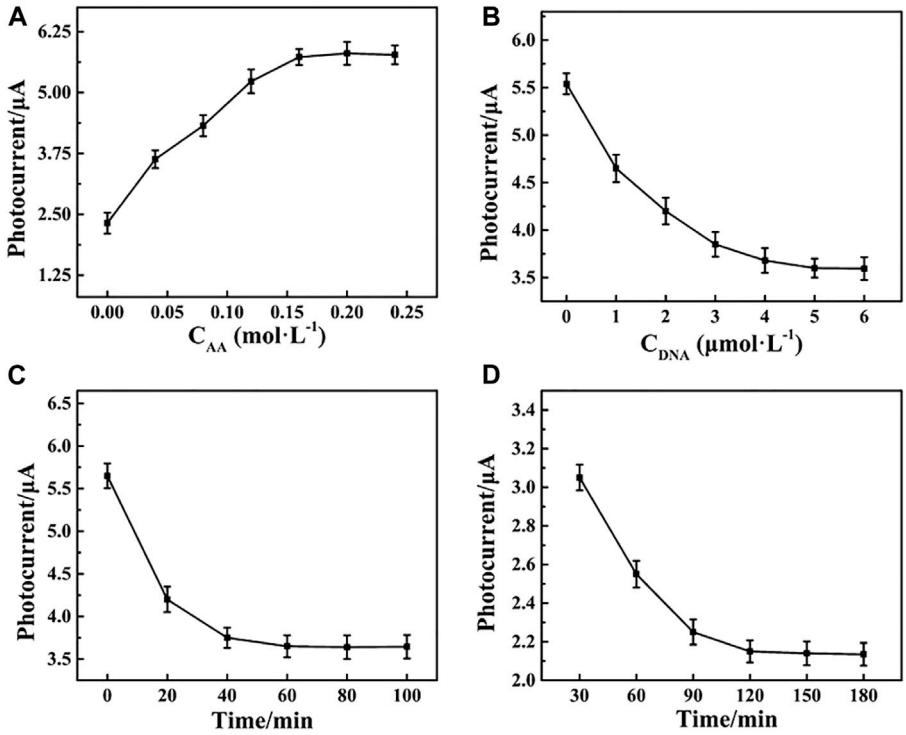

FIGURE 4
Effects of the **(A)** concentration of Apt-DNA, **(B)** amount of AA, **(C)** incubation time of the Apt-DNA with the photoelectrode, and **(D)** captured electrode with MCF-7 cells.

photocurrent due to steric hindrance. The evolution of the current signal could be reflected directly through the concentration of MCF-7 cells. The fabricated PEC aptasensor showed excellent sensitivity, stability, and selectivity. Additionally, MCF-7 cells in human serum were determined by this PEC aptasensor, which exhibited great potential in clinical detection.

2 Materials and methods

2.1 Materials and apparatus

Ferrous sulfate hydrate ($FeSO_4{\cdot}7H_2O$), urea, ethanol, ammonium molybdate tetrahydrate ($(NH_4)_6MoO_{24}{\cdot}4H_2O$), thiourea, bismuth nitrate pentahydrate ($Bi(NO_3)_3{\cdot}5H_2O$), glacial acetic acid, glutaraldehyde (50%, GA), ascorbic acid (AA), isopropanol (IPA), p-benzoquinone (BQ), methylene blue (MB), and chitosan (CS) were purchased from Aladdin Reagent Company (Shanghai, China). Fluorine-doped tin oxide (FTO) glass was obtained from South China Xiangcheng Technology Co., Ltd. Oligonucleotides and bovine serum albumin (BSA) were purchased from Sangon Biotech Co., Ltd. (Shanghai, China), and all chemical reagents were analytical grade without further purification.

Aptamer DNA (Apt-DNA):

$NH_2 - C_{12}$–CACTACAGAGGTTGCGTCTGTCCCACGTTGTCA
TGGG GGGTTGGCCTG

All the electrochemical measurements were carried out on a CHI 760E electrochemical workstation (Shanghai Chenhua Instrument Co., Ltd., China) with a three-electrode system composed of FTO as the working electrode, a platinum electrode as the counter electrode, and a saturate Ag/AgCl electrode as the reference electrode. Electrochemical impedance spectroscopy (EIS) and cyclic voltammetry (CV) were performed in 5 mM $K_3Fe(CN)_6$/$K_4Fe(CN)_6$ (0.1 M KCl) as the supporting electrolyte.

2.2 Preparation of the double Z-scheme α-Fe_2O_3/MoS_2/Bi_2S_3 ternary heterojunction

Flower-like α-Fe_2O_3 with nanorod petals was prepared as depicted in a previous report with minor modification (Wang et al., 2023c). First, 2.28 g of $FeSO_4{\cdot}7H_2O$ and 0.6 g of urea were dissolved in 100 mL mixed solution (V_{H2O}:V_{C2H5OH} = 4:1) and sonicated for 10 min. Then, the mixed solution was transferred into a 250-mL three-necked flask to reflux at 90°C for 6 h. After precipitation and drying at 60°C for 24 h, the reddish brown FeOOH powder was prepared. Subsequently, the α-Fe_2O_3 nanorods were obtained by the calcination of the prepared FeOOH at 500°C for 3 h in a Laboratory Muffle stove.

α-Fe_2O_3/MoS_2 nanocomposites were successfully prepared via a hydrothermal route. First, 0.1234 g of $(NH_4)_6MoO_{24}{\cdot}4H_2O$ and 0.2284 g of thiourea were dissolved in 35 mL of distilled water and stirred for 30 min. Then, 0.357 g of α-Fe_2O_3 was added to the above solution under stirring for 30 min. Subsequently, the

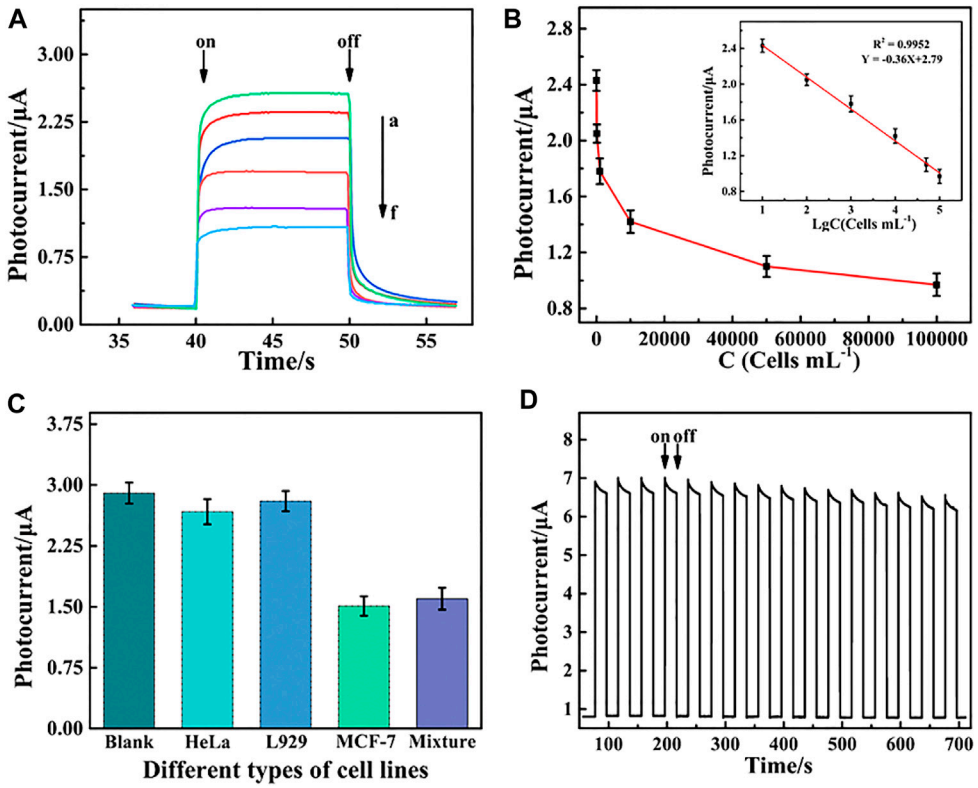

FIGURE 5
(A) Photocurrent responses of the PEC aptasensor toward MCF-7 cells and **(B)** relationship of the PEC signal and cell concentration at different concentrations ranging from 10 to 1x10^5 cells mL^{-1}. Inset of **(B)** shows linear relationship between the change in photocurrent intensity (ΔI) and the logarithm value of the MCF-7 cell concentration. **(C)** Selectivity of PEC detection for MCF-7 cells including the blank, HeLa, L929, MCF-7 cells, and mixture cells containing HeLa, L929, and MCF-7. **(D)** Stability of the PEC biosensor under repeated light irradiation from 0 to 700 s.

TABLE 1 Comparison of the performance of the PEC aptasensor with other methods for CTC detection.

Method	Linear range	Detection limit	Reference
Electrochemistry	18–1.5 × 10^6 cells/ mL^{-1}	6 cells/ mL^{-1}	Zhang et al. (2020b)
PEC	10^2–5 × 10^5 cells/ mL^{-1}	15 cells/ mL^{-1}	Ding et al. (2023)
Fluorescence	10–10^5 cells/ mL^{-1}	3 cells/ mL^{-1}	Chen et al. (2021)
Chemiluminescence	10^2–1 × 10^6 cells/ mL^{-1}	15 cells/ mL^{-1}	He et al. (2015)
Colorimetry	10^2–10^5 cells/ mL^{-1}	12 cells/ mL^{-1}	Wang et al. (2018)
This work	10–10^5 cells/ mL^{-1}	3 cells/ mL^{-1}	

obtained solution was transferred to a 50-mL Teflon-sealed autoclave and heated to 200°C for 6 h. After being cooled to room temperature, the α-Fe_2O_3/MoS_2 nanocomposites were obtained after being centrifuged and washed three times.

α-Fe_2O_3/MoS_2/Bi_2S_3 nanocomposites were successfully prepared by a hydrothermal process. First, 0.0236 g of thiourea was added in 25 mL distilled water and stirred for 3 min. Then, 0.076 g of $Bi(NO_3)_3{\cdot}5H_2O$ was added to the above solution and stirred for 20 min. Then, 0.04 g of α-Fe_2O_3/MoS_2 nanocomposites was added and stirred at 180°C for 20 min. After being cooled to room temperature, the α-Fe_2O_3/MoS_2/Bi_2S_3 nanocomposites were obtained after being centrifuged and washed. The product was dried in an oven at 60°C for 24 h for the next experiment.

2.3 Fabrication of the PEC aptasensor and PEC detection of CTCs

The PEC aptasensor based on a direct dual Z-scheme α-Fe_2O_3/MoS_2/Bi_2S_3 ternary heterojunction for the ultrasensitive detection of CTCs is shown in Scheme 1. First, 20 μL (2 mg mL^{-1}) of α-Fe_2O_3/MoS_2/Bi_2S_3 nanocomposites were dropped to the surface of FTO,

TABLE 2 Spiked detection of CTCs in serum samples (n = 6).

Add (cells mL^{-1})	Detected (cells mL^{-1})	Recovery (%)	RSD (%)
50	46	92	6.2
100	93	93	7.8
500	538	107.6	6.5
1,000	1,053	105.3	5.7

and 20 μL of mixture solution containing chitosan and acetic acid (chitosan/acetic acid = 1%, w/v) was added on the electrode surface of FTO/α-Fe_2O_3/MoS_2/Bi_2S_3. After being dried at 37°C, the FTO/α-Fe_2O_3/MoS_2/Bi_2S_3 electrode was immersed in GA solution (0.2%) and incubated for 30 min. Then, 20 μL of aptamer DNA (5 μM) was dropped onto the electrode and incubated for 40 min at 37°C. Subsequently, 20 μL of BSA (1%) was used to block the nonspecific binding sites, and the capture electrode FTO/α-Fe_2O_3/MoS_2/Bi_2S_3/CS/GA/BSA was constructed. A volume of 20 μL of MCF-7 cell solution with different concentrations was dropped onto the electrode surface and incubated for 120 min at 37°C. Finally, the PEC response of the biosensor was recorded in 10 mL of PBS (0.01 M, pH 7.4) containing ascorbic acid (AA, 0.14 mol L^{-1}) under visible light irradiation using a LED lamp (excitation wavelength, 450 nm; 100 W) with on–off light switching of 10 s.

3 Results and discussion

3.1 Characterization of the α-Fe_2O_3/MoS_2/Bi_2S_3 ternary heterojunction

SEM was used to analyze the morphology of the as-synthesized samples. As shown in Figure 1A, the SEM image of α-Fe_2O_3 displayed a uniform flower-like nanostructure, and the nanorod petal was approximately 3–4 μm in length. The SEM image of α-Fe_2O_3/MoS_2 (Figure 1B) revealed that α-Fe_2O_3 was encapsulated in MoS_2 nanosheets and exhibited ripples, which indicated the formation of the α-Fe_2O_3/MoS_2 heterojunction. Subsequently, Bi_2S_3 grew in the layered MoS_2, and the α-Fe_2O_3/MoS_2/Bi_2S_3 ternary heterojunction exhibited an icicle flower-like structure, as shown in Figure 1C. X-ray diffraction (XRD) patterns were used to characterize the α-Fe_2O_3/MoS_2/Bi_2S_3 ternary heterojunction. Figure 1D shows the characteristic diffraction peaks that correspond to the JCPDS card No. 33–0664 α-Fe_2O_3, respectively. Additionally, three peak representatives (14.13°, 28.47°, and 32.91°) which belonged to the (002), (004), and (100) crystal planes of MoS_2 (JCPDS card No. 75–1539), respectively, proved the formation of MoS_2. Meanwhile, a few prominent peaks of Bi_2S_3 appeared based on JCPDS card No. 17–0320. These illustrated the formation of the α-Fe_2O_3/MoS_2/Bi_2S_3 ternary heterojunction. As expected, the element mapping images (Figure 1E) showed the distribution of O, Bi, Mo, S, and Fe, offering direct evidence of the effective achievement of α-Fe_2O_3/MoS_2/Bi_2S_3 ternary heterojunction. The UV-vis absorption spectra of α-Fe_2O_3, α-Fe_2O_3/Bi_2S_3, and α-Fe_2O_3/MoS_2/Bi_2S_3 were investigated as described in Supplementary Figure S1. Both MoS_2 and Bi_2S_3 presented a broad absorption spectrum across the visible light region. For the α-Fe_2O_3/MoS_2/Bi_2S_3 heterojunction, α-Fe_2O_3 also enhanced its absorption ability in visible light, which would lead to an increase in photocatalytic activity.

3.2 Photocatalytic mechanism of the α-Fe_2O_3/MoS_2/Bi_2S_3 ternary heterojunction

The band gap energy (Eg) of α-Fe_2O_3 (2.1 eV), MoS_2 (1.38 eV), and Bi_2S_3 (1.41 eV) was investigated by UV–vis diffuse reflectance spectroscopy, and the flat-band potentials (α-Fe_2O_3, 0.69 eV; MoS_2, −0.4 eV; Bi_2S, 0.59 eV; all vs. SSCE) were derived using Mott–Schottky plots, as shown in Supplementary Figure S2. Their valence bands (VBs) were 0.93 eV, −0.16 eV, and −0.35 eV, respectively, which was obtained based on the following formula: VB = CB + Eg. The trapping experiments of reactive species in this photocatalytic process were carried out. In this work, IPA (radical •OH scavenger) and BQ (radical $\bullet O^{2-}$ scavenger) were employed as quenchers in the degradation experiment of methylene blue (MB), as shown in Supplementary Figure S3. During this photocatalytic process, both BQ and IPA significantly reduced the degradation rate of MB, demonstrating that a larger amount of •OH and $\bullet O^{2-}$ on the surface of α-Fe_2O_3/MoS_2/Bi_2S_3 was involved in the degradation of MB. The standard potential of the OH^-/•OH pair (+2.40 eV vs. NHE) was lower than the VB position of α-Fe_2O_3 and higher than the VB position of both MoS_2 and Bi_2S_3. We could speculate that only h+ of α-Fe_2O_3 reacted with OH− or H_2O to form •OH. Meanwhile, the standard potential of the O_2/$\bullet O^{2-}$pair (−0.33 eV vs. NHE) was more positive than that of Bi_2S_3 and more negative than the CB of both α-Fe_2O_3 and MoS_2. It was concluded that $\bullet O^{2-}$was more possible to be produced by Bi_2S_3.

Based on these, the transfer pathway of electrons in α-Fe_2O_3/MoS_2/Bi_2S_3 is shown in Figure 2. Under visible irradiation, photo-generated e−/h+ was produced on the CB and VB of α-Fe_2O_3, Bi_2S_3, and MoS_2. The e− in the CB of α-Fe_2O_3 and MoS_2 transferred to the VB of MoS_2 and Bi_2S_3 to recombine with the h+, respectively. This resulted in the accumulation of high-energy e− and h + on the VB of Bi_2S_3 and the CB of α-Fe_2O_3, where they participated in photocurrent production. This double Z-scheme heterojunction promoted the detecting photocurrent intensity in the PEC aptasensor because it effectively inhibited the recombination of electron–hole pairs and absorbed sufficient light.

3.3 Characterization of the PEC aptasensor

As shown in Figure 3A, the photocurrent of FTO/α-Fe_2O_3/MoS_2/Bi_2S_3 (curve b) was much larger than that of the naked FTO electrode (curve a) due to the creation of ternary heterojunctions with high light absorption and photoelectric conversion efficiency. Steric hindrance caused a reduction in photocurrents after Apt-DNA (curve c), BSA (curve d), and MCF-7 cell (curve e) were assembled on the photoelectrode of FTO/α-Fe_2O_3/MoS_2/Bi_2S_3. These demonstrated that the PEC aptasensor was successfully

constructed. Meanwhile, electrochemical impedance spectroscopy (EIS) was also carried out to validate this process. The diameter of the high-frequency semicircle in the Nyquist plot corresponded to the electron transfer resistance (R_{et}) of the electrode surface (Luo et al., 2022). As shown in Figure 3B, the R_{et} value of the naked FTO electrode was small (curve a), and it drastically decreased (curve b) when the α-Fe_2O_3/MoS_2/Bi_2S_3 heterojunction was dropped on the FTO electrode. Subsequently, when the Apt-DNA (curve c), BSA (curve d), and MCF-7 cell (curve e) were continuously assembled on the FTO/α-Fe_2O_3/MoS_2/Bi_2S_3 surface, they led to an increase in R_{et} because they impeded the diffusion of electrons to the electrode surface, indicating their successful immobilization.

3.4 Optimization of PEC measurement conditions

A number of parameters, including the concentration of Apt-DNA, the amount of AA, and the incubation time of the Apt-DNA with the photoelectrode and captured electrode with MCF-7 cells, were optimized. As shown in Figure 4A, the photocurrent response peaked at 0.15 mol L^{-1}, and no obvious change was observed at higher concentrations. As a result, the concentration of AA in all subsequent experiments was 0.15 mol L^{-1}. The impact of Apt-DNA concentration on the PEC response of the biosensor is shown in Figure 4B. The photocurrent decreased as the concentration of Apt-DNA increased up to 5 M, after which there was no obvious change, indicating Apt-DNA saturation. Accordingly, 5 μM of Apt-DNA was used in all subsequent experiments. The immobilization time is also shown in Figure 4C. The photocurrent decreased in the range from 0 to 60 min and then remained constant. It was that the amount of Apt-DNA was saturated after a certain time. Meanwhile, the incubation time of Apt-DNA with the captured electrode was also examined, as shown in Figure 4D. The ideal duration was found to be approximately 120 min. Under optimal conditions, the photocurrent was large and stable, which would be performed for subsequent experiments.

3.5 Detection performance of the PEC aptasensor

The PEC response decreased with an increase in MCF-7 cell concentrations due to steric hindrance (Figure 5A). The decrease in photocurrent intensity demonstrated a good linear relationship with the logarithm of the MCF-7 cell concentration in the range from 10 to 1×10^5 cells mL^{-1} (Figure 5B). The linear regression equation was y = −0.36 lgC cells+2.79 (C cells, cell mL^{-1}) with a correlation coefficient (R^2) of 0.9952 (n = 3) and a low detection limit of 3 cell mL^{-1} (S/N = 3). Therefore, the PEC aptasensor exhibited an ultrasensitive detection of MCF-7 cells compared with the other biosensors given in Table 1.

3.6 Application of the PEC aptasensor in real samples

To assess the application potential, the prepared PEC aptasensor was used to detect MCF-7 cells in real samples. MCF-7 cells with different concentrations (10, 50, 100, 500, and 1,000 cells mL^{-1}) were spiked into serum samples for the assay. The recoveries of MCF-7 were between 92% and 107.6% with a relative standard deviation (RSD) from 5.7% to 7.8% (Table 2), demonstrating great potential for the detection of CTCs in real samples.

4 Conclusion

In summary, we developed a dual Z-scheme PEC aptasensor based on the α-Fe_2O_3/MoS_2/Bi_2S_3 ternary heterojunction for the ultrasensitive detection of CTCs. The α-Fe_2O_3/MoS_2/Bi_2S_3 ternary nanocomposite was prepared via a step-by-step route, and the analysis of radical trapping experiments confirmed that the active species $\bullet O^{2-}$, h^+, and •OH were produced in the α-Fe_2O_3/MoS_2/Bi_2S_3 photocatalytic system. The mechanism analysis demonstrated that the charge transfer of the α-Fe_2O_3/MoS_2/Bi_2S_3 nanocomposite followed a dual Z-scheme route, which exhibited a significant enhanced photocurrent under visible light, resulting in improved visible light absorption, increased surface area, and enhanced separation efficiency of photo-generated electron–hole pairs. The constructed PEC aptasensor offered a linear PEC response, with the CTC concentration ranging from 10 to 1×10^5 cells mL^{-1} and a low detection limit of 3 cell mL^{-1} (S/N = 3). Additionally, MCF-7 cells in human serum were determined by this PEC aptasensor, which exhibited great potential in clinical detection.

Data availability statement

The original contributions presented in the study are included in the article/Supplementary Material; further inquiries can be directed to the corresponding authors.

Author contributions

KF: conceptualization, formal analysis, and writing–original draft. YD: investigation, methodology, and writing–review and editing. MH: project administration, supervision, and writing–original draft. WY: conceptualization, project administration, and writing–original draft. YG: data curation, formal analysis, and writing–original draft. XH: project administration, supervision, and writing–review and editing. YW: writing–original draft and writing–review and editing.

Funding

The author(s) declare that financial support was received for the research, authorship, and/or publication of this article. This research was funded by the National Natural Science Foundation of China (No. 81802372), Hebei Natural Science Foundation (H2020107005 and H2020107002), and the Scientific and Technological Project of the Hebei Province of China (No. 14397702D).

Conflict of interest

The authors declare that the research was conducted in the absence of any commercial or financial relationships that could be construed as a potential conflict of interest.

Publisher's note

All claims expressed in this article are solely those of the authors and do not necessarily represent those of their affiliated organizations, or those of the publisher, the editors, and the reviewers. Any product that may be evaluated in this article, or claim that may be made by its manufacturer, is not guaranteed or endorsed by the publisher.

Supplementary material

The Supplementary Material for this article can be found online at: https://www.frontiersin.org/articles/10.3389/fbioe.2024.1372688/full#supplementary-material

References

Chen, P., Wang, Y., He, Y., Huang, K., Wang, X., Zhou, R., et al. (2021). Homogeneous visual and fluorescence detection of circulating tumor cells in clinical samples via selective recognition reaction and enzyme-free amplification. *ACS Nano* 15, 11634–11643. doi:10.1021/acsnano.1c02080

Den Toonder, J. (2011). Circulating tumor cells: the grand challenge. *Lab a Chip* 11, 375–377. doi:10.1039/c0lc90100h

Ding, Z., Lin, Q., Xu, X., Tang, X., Zhang, X., Li, W., et al. (2023). High-performance assay of HepG2 cells through inertial separation in a microfluidic chip coupled with fluorescence and photoelectrochemical detection. *Sensors Actuators B Chem.* 392, 134054. doi:10.1016/j.snb.2023.134054

Dirix, L., Elst, H., Benoy, I., Van der Auwera, I., Prové, A., Wuyts, H., et al. (2009). Circulating tumor cell detection: a direct comparison between the CellSearch system, the AdnaTest, and CK-19/mammaglobin RT-PCR in patients with metastatic breast cancer. *J. Clin. Oncol.* 27, e22117. doi:10.1200/jco.2009.27.15_suppl.e22117

Fang, X., and Tan, W. (2010). Aptamers generated from cell-SELEX for molecular medicine: a chemical biology approach. *Acc. Chem. Res.* 43, 48–57. doi:10.1021/ar900101s

Freeman, R., Girsh, J., and Willner, I. (2013). Nucleic acid/quantum dots (QDs) hybrid systems for optical and photoelectrochemical sensing. *ACS Appl. Mater. Interfaces* 5, 2815–2834. doi:10.1021/am303189h

Gong, L., Cretella, A., and Lin, Y. (2023). Microfluidic systems for particle capture and release: a review. *Biosens. Bioelectron.* 236, 115426. doi:10.1016/j.bios.2023.115426

Guo, M., Xing, Z., Zhao, T., Qiu, Y., Tao, B., Li, Z., et al. (2020). Hollow flower-like polyhedral α-Fe2O3/Defective MoS2/Ag Z-scheme heterojunctions with enhanced photocatalytic-Fenton performance via surface plasmon resonance and photothermal effects. *Appl. Catal. B Environ.* 272, 118978. doi:10.1016/j.apcatb.2020.118978

Han, Q., Wang, R., Xing, B., Chi, H., Wu, D., and Wei, Q. (2018). Label-free photoelectrochemical aptasensor for tetracycline detection based on cerium doped CdS sensitized BiYWO6. *Biosens. Bioelectron.* 106, 7–13. doi:10.1016/j.bios.2018.01.051

He, Y., Li, J., and Liu, Y. (2015). Reusable and dual-potential responses electrogenerated chemiluminescence biosensor for synchronously cytosensing and dynamic cell surface N-glycan evaluation. *Anal. Chem.* 87, 9777–9785. doi:10.1021/acs.analchem.5b02048

Hong, B., and Zu, Y. (2013). Detecting circulating tumor cells: current challenges and new trends. *Theranostics* 3, 377–394. doi:10.7150/thno.5195

Hong, X., Kim, J., Shi, S.-F., Zhang, Y., Jin, C., Sun, Y., et al. (2014). Ultrafast charge transfer in atomically thin MoS2/WS2 heterostructures. *Nat. Nanotechnol.* 9, 682–686. doi:10.1038/nnano.2014.167

Jiang, L., Yuan, X., Zeng, G., Liang, J., Chen, X., Yu, H., et al. (2018). *In-situ* synthesis of direct solid-state dual Z-scheme WO3/g-C3N4/Bi2O3 photocatalyst for the degradation of refractory pollutant. *Appl. Catal. B Environ.* 227, 376–385. doi:10.1016/j.apcatb.2018.01.042

Li, Y., Wang, H., Xie, L., Liang, Y., Hong, G., and Dai, H. (2011). MoS2 nanoparticles grown on graphene: an advanced catalyst for the hydrogen evolution reaction. *J. Am. Chem. Soc.* 133, 7296–7299. doi:10.1021/ja201269b

Liu, Y., Shi, Y., Liu, X., and Li, H. (2017). A facile solvothermal approach of novel Bi2S3/TiO2/RGO composites with excellent visible light degradation activity for methylene blue. *Appl. Surf. Sci.* 396, 58–66. doi:10.1016/j.apsusc.2016.11.028

Luo, J., Zeng, Q., Liu, S., Wei, Q., Wang, Z., Yang, M., et al. (2022). Highly sensitive photoelectrochemical sensing platform based on PM6: Y6 pn heterojunction for detection of MCF-7 cells. *Sensors Actuators B Chem.* 363, 131814. doi:10.1016/j.snb.2022.131814

Osterloh, F. E. (2013). Inorganic nanostructures for photoelectrochemical and photocatalytic water splitting. *Chem. Soc. Rev.* 42, 2294–2320. doi:10.1039/c2cs35266d

Pei, J., Yang, J., Yildirim, T., Zhang, H., and Lu, Y. (2019). Many-body complexes in 2D semiconductors. *Adv. Mater.* 31, 1706945. doi:10.1002/adma.201706945

Saravanakumar, K., and Park, C. M. (2021). Rational design of a novel LaFeO3/g-C3N4/BiFeO3 double Z-scheme structure: photocatalytic performance for antibiotic degradation and mechanistic insight. *Chem. Eng. J.* 423, 130076. doi:10.1016/j.cej.2021.130076

Stoltenburg, R., Reinemann, C., and Strehlitz, B. (2007). SELEX—a (r)evolutionary method to generate high-affinity nucleic acid ligands. *Biomol. Eng.* 24, 381–403. doi:10.1016/j.bioeng.2007.06.001

Tang, M., Wen, C.-Y., Wu, L.-L., Hong, S.-L., Hu, J., Xu, C.-M., et al. (2016). A chip assisted immunomagnetic separation system for the efficient capture and *in situ* identification of circulating tumor cells. *Lab a Chip* 16, 1214–1223. doi:10.1039/c5lc01555c

Van der Auwera, I., Peeters, D., Benoy, I., Elst, H., Van Laere, S., Prove, A., et al. (2010). Circulating tumour cell detection: a direct comparison between the CellSearch System, the AdnaTest and CK-19/mammaglobin RT–PCR in patients with metastatic breast cancer. *Br. J. cancer* 102, 276–284. doi:10.1038/sj.bjc.6605472

Wang, J., Gao, Z., Dong, M., Li, J., Jiang, H., Xu, J., et al. (2023a). CdSe@CdS quantum dot–sensitized Au/α-Fe2O3 structure for photoelectrochemical detection of circulating tumor cells. *Microchim. Acta* 190, 221. doi:10.1007/s00604-023-05797-w

Wang, J., Gao, Z., Dong, M., Li, J., Jiang, H., Xu, J., et al. (2023c). CdSe@ CdS quantum dot–sensitized Au/α-Fe2O3 structure for photoelectrochemical detection of circulating tumor cells. *Microchim. Acta* 190, 221. doi:10.1007/s00604-023-05797-w

Wang, Q., Ren, C., Zhao, Y., Fang, F., Yin, Y., Ye, Y., et al. (2023b). Photocatalytic pollutant elimination and hydrogen production over TiO2 NTs/Bi2S3-MoS2 with Z-scheme configuration: kinetics and mechanism. *Mater. Res. Bull.* 167, 112430. doi:10.1016/j.materresbull.2023.112430

Wang, W., Liu, S., Li, C., Wang, Y., and Yan, C. (2018). Dual-target recognition sandwich assay based on core-shell magnetic mesoporous silica nanoparticles for sensitive detection of breast cancer cells. *Talanta* 182, 306–313. doi:10.1016/j.talanta.2018.01.067

Wheeler, D. A., Wang, G., Ling, Y., Li, Y., and Zhang, J. Z. (2012). Nanostructured hematite: synthesis, characterization, charge carrier dynamics, and photoelectrochemical properties. *Energy and Environ. Sci.* 5, 6682–6702. doi:10.1039/c2ee00001f

Wu, S., Huang, H., Shang, M., Du, C., Wu, Y., and Song, W. (2017). High visible light sensitive MoS2 ultrathin nanosheets for photoelectrochemical biosensing. *Biosens. Bioelectron.* 92, 646–653. doi:10.1016/j.bios.2016.10.037

Yang, D., Liu, M., Xu, J., Yang, C., Wang, X., Lou, Y., et al. (2018). Carbon nanosphere-based fluorescence aptasensor for targeted detection of breast cancer cell MCF-7. *Talanta* 185, 113–117. doi:10.1016/j.talanta.2018.03.045

Yi, K., Kong, H., Lao, Y. H., Li, D., Mintz, R. L., Fang, T., et al. (2023). Engineered nanomaterials to potentiate CRISPR/Cas9 gene editing for cancer therapy. *Adv. Mater.* 2023, 2300665. doi:10.1002/adma.202300665

Yu, Y., Wu, K., Xu, W., Chen, D., Fang, J., Zhu, X., et al. (2021). Adsorption-photocatalysis synergistic removal of contaminants under antibiotic and Cr (VI) coexistence environment using non-metal g-C3N4 based nanomaterial obtained by supramolecular self-assembly method. *J. Hazard. Mater.* 404, 124171. doi:10.1016/j.jhazmat.2020.124171

Yue, Z., Lisdat, F., Parak, W. J., Hickey, S. G., Tu, L., Sabir, N., et al. (2013). Quantum-dot-based photoelectrochemical sensors for chemical and biological detection. *ACS Appl. Mater. interfaces* 5, 2800–2814. doi:10.1021/am3028662

Zhang, H., Liang, F., Wu, X., Liu, Y., and Chen, A. (2020b). Recognition and sensitive detection of CTCs using a controllable label-free electrochemical cytosensor. *Microchim. Acta* 187, 487. doi:10.1007/s00604-020-04452-y

Zhang, Z., Nagashima, H., and Tachikawa, T. (2020a). Ultra-narrow depletion layers in a hematite mesocrystal-based photoanode for boosting multihole water oxidation. *Angew. Chem. Int. Ed.* 59, 9047–9054. doi:10.1002/anie.202001919

Zhao, M., Wang, R., Yang, K., Jiang, Y., Peng, Y., Li, Y., et al. (2023). Nucleic acid nanoassembly-enhanced RNA therapeutics and diagnosis. *Acta Pharm. Sin. B* 13, 916–941. doi:10.1016/j.apsb.2022.10.019

Zhong, S., Chen, L., Shi, X., Chen, G., Sun, D., and Zhang, L. (2023). Recent advances in electrochemical aptasensors for detecting cardiac biomarkers: a review. *Microchem. J.* 193, 109063. doi:10.1016/j.microc.2023.109063